

A Systematic Study of Planetary Envelope Growth with 3D Radiation-Hydrodynamics Simulations

AVERY BAILEY,^{1,2} JAMES M. STONE,^{3,4} AND JEFFREY FUNG⁵

¹*Department of Physics and Astronomy, University of Nevada, Las Vegas, 4505 South Maryland Parkway, Las Vegas, NV 89154-4002, USA*

²*Nevada Center for Astrophysics (NCfA), University of Nevada, Las Vegas, NV, USA*

³*School of Natural Sciences, Institute for Advanced Study, Princeton, NJ 08544, USA*

⁴*Department of Astrophysical Sciences, Princeton University, Princeton, NJ 08544, USA*

⁵*Department of Physics & Astronomy, Clemson University, SC 29634, USA*

ABSTRACT

In the core accretion model of planet formation, envelope cooling regulates the accretion of material and ultimately sets the timescale to form a giant planet. Given the diversity of planet-forming environments, opacity uncertainties, and the advective transport of energy by 3-dimensional recycling flows, it is unclear whether 1D models can adequately describe envelope structure and accretion in all regimes. Even in 3D models, it is unclear whether approximate radiative transfer methods sufficiently model envelope cooling particularly at the planetary photosphere. To address these uncertainties, we present a suite of 3D radiation hydrodynamics simulations employing methods that directly solve the transfer equation. We perform a parameter space study, formulated in terms of dimensionless parameters, for a variety of envelope optical depths and cooling times. We find that the thermodynamic structure of the envelope ranges from adiabatic to isothermal based on the cooling time and by extension, the background disk temperature and density. Our models show general agreement with 1D static calculations, suggesting a limited role of recycling flows in determining envelope structure. By adopting a dimensionless framework, these models can be applied to a wide range of formation conditions and assumed opacities. In particular, we dimensionalize them to the case of a super-Earth and proto-Jupiter and place upper limits on the 3D mass accretion rates prior to runaway growth. Finally, we evaluate the fidelity of approximate radiative transfer methods and find that even in the most challenging cases, more approximate methods are sufficiently accurate and worth their savings in computational cost.

Keywords: planets and satellites: formation — radiative transfer — planets and satellites: gaseous planets — planets and satellites: interiors

1. INTRODUCTION

Because the growth of planetary envelopes is regulated by cooling, an adequate treatment of radiative processes is necessary for any comprehensive model of planet formation. In this section, we improve our planetary envelope models by including radiative transfer. Unlike our previous isothermal models, this allows us to study the accretion process and quasi-static contraction of the envelope. 1D models of core accretion predict various accretion rates that are then used as the inputs for population synthesis models and compared to exoplanet statistics. While these models are good in the sense that

robustly produce giants at intermediate distances, they are not perfect and tend to under-produce intermediate mass planets, close-in super-Earths, and giants at extended distances. This suggests some problem with the underlying assumptions or a currently unaccounted piece of physics. Because the inputs are based upon scaling laws and solutions obtained from 1D quasi-static models, it is worthwhile to ask whether the same results are obtained from 3D hydrodynamics models. While this is not the first study to do so (Ayliffe & Bate 2009, 2012; Schulik et al. 2019; Lambrechts et al. 2019), few studies focus on the low mass $\sim 10M_{\oplus}$ regime. The studies that do (D’Angelo & Bodenheimer 2013; Lambrechts & Lega 2017), recover something similar to 1D models but tend to focus on a small number of tailored models and employ flux-limited diffusion for the radia-

tive transfer (the exception being [Zhu et al. \(2021\)](#)). Because cooling and consequently mass accretion is determined by the radiative transfer, flux-limited diffusion may not be appropriate in all cases. For these reasons, we find it worthwhile to examine the cooling of low mass planets with accurate radiative transfer and also a wider parameter space. Because we are interested in the formation of a diversity of planets at all manner of distances, we will formulate a more agnostic dimensionless approach that is more suitable than running just a $10M_{\oplus}$ Jupiter core at 5 AU.

These simulations will also be useful for testing various thermodynamic assumptions adopted by 3D hydrodynamics studies. In the simplest cases, an isothermal or adiabatic equation of state is adopted. Lacking radiative cooling, these simulations quickly arrive at a steady state, making for a convenient study of the time-independent flow field and associated envelope structure ([Fung et al. 2015](#); [Ormel et al. 2015](#); [Fung et al. 2019](#)). Our radiative simulations are able to cool and therefore should fall somewhere in between the adiabatic and isothermal cases. With our simulations, we can measure how isothermal or adiabatic a given envelope is and define regions of parameter space where these simple thermodynamic assumptions are approximately satisfied. Because the adopted thermodynamics are linked to kinematic properties of the planet’s envelope and things like CPD formation ([Fung et al. 2019](#)), this association will also help map the kinematic features of planetary envelopes into the space of models with realistic cooling.

Our radiative models will also test the validity of cooling models that go beyond the simple adiabatic/isothermal assumption. Some models for example [Kurokawa & Tanigawa \(2018\)](#), opt for a simple Newtonian-like cooling prescription. This is a computationally expedient cooling implementation and useful for constructing toy models of planet growth, but it is not self-consistent or physically realistic and will fail in regimes to which it is not tuned. Other studies adopt flux-limited diffusion for including radiative effects in 3D planet simulations ([D’Angelo & Bodenheimer 2013](#); [Cimerman et al. 2017](#); [Szulágyi 2017](#); [Lambrechts & Lega 2017](#)). While FLD is convenient for adding minimal computational cost and is accurate in the diffusion limit, it adopts a heuristic to limit the flux in optically thin regimes. Because of this, the method is poorly suited for determining radiation fluxes at intermediate $\tau \sim 1$ optical depths. Being a diffusion approximation, it also assumes that the radiative flux is always aligned with the temperature gradient, an assumption at odds with the free-streaming of radiation in optically thin re-

gions. These shortcomings have spurred some interest in applying higher order moment methods like M1 to the study of planet formation ([Melon Fuksman et al. 2021](#)). Because we have implemented radiative methods into ATHENA++ that solve the actual discretized transfer equation, our planet models here should test the fidelity of these more widely used approximate methods. While this is not the primary motivation for this study, it should help to inform future studies about the relative cost-benefit in moving to more accurate methods of radiation transfer.

The primary goal of this paper is to detail and test the fidelity of the method while presenting some properties of the envelope models themselves. More physically motivated applications of these models are and will be the subject of additional papers ([Zhu et al. 2023](#); [Bailey & Zhu 2023](#)). We begin the rest of this chapter by describing simulation details specific to the inclusion of radiative transfer. This includes the definition of dimensionless parameters used to characterize our radiative models. We then thoroughly investigate a single proto-Jupiter model to develop an understanding for a prototypical radiative model and also act as a test-bed for numerical subtleties. The following section expands upon this single model by exploring a wider parameter space under different assumed opacities and disk conditions.

2. SIMULATION DETAILS

The appropriate equations to model 3D envelope evolution are the hydrodynamics equations supplemented by source terms due to gravity, rotational motion, and radiative cooling. To good approximation, a static form of the radiative transfer equations can be used, where terms of order v/c or higher are neglected. In a dimensionless form with length scale $H_0 \equiv \sqrt{kT_0/\mu m_p}$, timescale $1/\Omega_0 \equiv \sqrt{a^3/GM_*}$, and density scale ρ_0 , the equations solved (with coriolis and centrifugal source term omitted for notational ease) are:

$$\frac{\partial \rho}{\partial t} + \nabla \cdot (\rho v) = 0 \quad (1)$$

$$\frac{\partial (\rho v)}{\partial t} + \nabla \cdot (\rho v \otimes v + p) = -\rho \nabla \Phi \quad (2)$$

$$\frac{\partial E}{\partial t} + \nabla \cdot (Ev + pv) = -\rho v \cdot \nabla \Phi + \rho \kappa \beta (J - S) \quad (3)$$

$$\frac{\partial I}{\partial s} = \rho \kappa (S - I) \quad (4)$$

where

$$E = \frac{p}{\gamma - 1} + \frac{1}{2}\rho v^2 \quad (5)$$

$$J = \frac{1}{4\pi} \int I d\Omega \quad (6)$$

$$S = \left(\frac{P}{\rho}\right)^4 \quad (7)$$

This particular form makes a number of assumptions including an LTE Planck source function, single (gray) absorption opacity. To solve the radiation-hydrodynamics equations, we use the short characteristics (SC) method (Kunasz & Auer 1988; Auer & Paletou 1994) identical to that of Davis et al. (2012). We also employ a local approximation and perform our simulations in a Cartesian coordinate system centered on the planet. Code units are taken by setting $H_0 = \Omega_0 = \rho_0 = 1$, reflecting the above choice of dimensionless equations. With this setup, all models have the same initial equilibrium state: $\rho = p = \exp(-z^2/2)$, and a y -velocity shear in \hat{x} . This equilibrium holds for both an adiabatic and isothermal equation of state, so long as no planet is introduced. With radiative transfer, the incident intensity at each boundary is fixed to the value of the initial source function (unity in code units) so that with no planet, the disk exists in radiative equilibrium. Physically this incident intensity can represent irradiation by the star or upper layers of the protoplanetary disk. In the future, the multi-frequency capabilities of the code could be leveraged to treat the incident radiation as ultraviolet but for now we limit ourselves to the single frequency irradiated case. With an initial equilibrium state, we introduce the planetary potential and investigate the resultant evolution under the influence of radiative cooling. This is contrived in the sense that real planets are not “suddenly introduced”, they evolve in conjunction with the disk throughout the formation process. Nevertheless, this methodology is consistent with other radiative-hydro simulations (Ayliffe & Bate 2012; D’Angelo & Bodenheimer 2013; Cimerman et al. 2017; Lambrechts & Lega 2017).

To make the potential parameter space more tenable, we adopt fixed values of $\mu = 2.3$ and $\gamma = 1.4$ between our models. With μ and γ fixed, 4 dimensionless parameters remain to uniquely characterize a given model. Two of these, thermal mass q_t and softening length ϵ are contained within the adopted form for gravity:

$$\Phi = \frac{GM_p}{\sqrt{r^2 + \epsilon^2}} \left(\frac{1}{\Omega_0^2 H_0^2} \right) = \frac{q_t}{\sqrt{(r/H_0)^2 + (\epsilon/H_0)^2}} \quad (8)$$

Whereas q_t is a parameter with physical significance, ϵ is less physical, arising partially out of numerical necessity.

For another dimensionless parameter, we have defined β . Defined as

$$\beta \equiv \frac{ac \left(\frac{\mu m_p}{k} \right) \frac{T_0^3}{\rho_0}}{c_s} \sim \frac{c_\gamma}{c_s} \quad (9)$$

is roughly the ratio of the characteristic velocity of photon diffusion c_γ relative to the disk sound speed c_s . A fourth dimensionless parameter enters through the choice of opacity law. Our models will assume a constant opacity κ_0 , so that the dimensionless opacity is simply

$$\kappa = \kappa_0 \rho_0 H_0 \approx \kappa_0 \Sigma_0, \quad (10)$$

and is therefore roughly the disk’s vertical optical depth. With these four dimensionless parameters, q_t , ϵ , β , κ , a given model can be uniquely expressed. This use of dimensionless parameters will simplify the discussion of planet formation when it comes to comparing models representing different planet-forming environments. We note that this whole methodology and creation of 4 dimensionless parameters neglects several potential pieces of microphysics that would otherwise add to the complexity of the models here. For example, we neglect ionization and molecular dissociation of Hydrogen which can change the equation of state and serve as an energy sink. While these are important, they are higher order corrections to our models especially in the context of our overly simple constant opacity assumption.

3. A PROTO-JUPITER MODEL ($\beta = 1$, $\kappa = 100$)

With the model details defined, we focus on a prototypical simulation of a Jupiter-like core under reasonable conditions at 5 AU in a protoplanetary disk. For this model we adopt the dimensionless parameters $q_t = 0.5$, $\beta = 100$, $\kappa = 1$ which corresponds to roughly a $10M_\oplus$ core orbiting at 5 AU around a solar mass star in a disk with background temperature $T_0 = 70$ K, integrated surface density $\Sigma_0 = 250$ g/cm², and opacity $\kappa_0 = 1$ cm²/g. With this opacity, the entirety of the Bondi sphere is optically thick, with the photosphere occurring near the vertical boundary of our simulation box at $2H_0$. This choice of parameters also corresponds to scale height aspect ratio of $h_p = 0.04$ at 5 AU. For now, we set the gravitational softening length at $\epsilon = 0.1R_b$, comparable to similar studies (Lambrechts & Lega 2017; Lambrechts et al. 2019; Schulik et al. 2019).

Though we have championed the short characteristics implementation of radiative transfer in Section 2, the transition to a regime in which this method starts to become computationally inefficient coincides with proto-Jupiter conditions. For this reason, our fiducial model in this section is performed with the method of Jiang (2021). We note that the method of Jiang (2021) is not

solving the same equations as those in Section 2 as it retains velocity dependent terms in the Lorentz transformation for the radiation. In the low-velocity limit, of course, this method does reduce to our static limit. For notational purpose we will sometimes refer to the Jiang (2021) as the ‘implicit’ method and SC as ‘explicit’ referring to the manner in which the transfer equation is solved.

For this proto-Jupiter case, we do run an additional SC model (albeit for fewer orbits) and confirm that the two radiation schemes return nearly indistinguishable results. Our fiducial model is run for 15 orbits and adopts a generous angular discretization of 12 angles per octant. We use two levels of mesh refinement so that the highest resolution attained is 128 cells/ R_b and the softening length is resolved by 12 cells. With these fiducial parameters, a simulation takes roughly 6000 core-hours to run 15 orbits. While mesh refinement makes it easy to increase the resolution without needing to add many more processors, more refinement levels also leads to more iterations of the radiation solver. This is because each processor solves its own local radiation problem on a part of the mesh and then communicates and iterates with other processors until a good enough global solution is found. Also, because the gravitational acceleration scales rather steeply with the softening length, it tends to be hard to get converged results for small softening length. For these reasons, in this work we focus on studying a number of models we trust are converged rather than 1-2 expensive high resolution models subject to more uncertainty.

The simulation begins from equilibrium with the introduction of the planetary potential. This triggers a rapid infall of gas as the atmosphere attempts to establish a pressure gradient in response and arrive at a new equilibrium. Within a single orbit, a spherically symmetric envelope forms around the planet and an approximate hydrostatic equilibrium is attained. Gas that has fallen into the planetary potential is heated, giving the envelope a temperature gradient. Due to the influence of radiative cooling, the temperature gradient is not as severe as an adiabatic profile. The gas is heated to only several times the background disk temperature because of our large softening length and absence of heating sources. In analytic models, this outer part of the planetary envelope is typically regarded as isothermal (Rafikov 2006; Piso & Youdin 2014), reflecting the modest temperature increase in this model.

After reaching a state of near hydrostatic equilibrium, the envelope cools radiatively and the temperature profile falls monotonically with time. This cooling leads to departures from spherical symmetry in the envelope

structure. Near the midplane, cool spiral substructures appear, aligned with the boundary between outgoing horseshoe flows and background shear flows. These departures from spherical symmetry can be seen in Fig. 1 where we plot snapshots of the midplane temperature distribution at different times in the fiducial simulation. While spiral arms are generic for planets irrespective of their thermodynamics, these cooled substructures only appear in radiative models. Furthermore, these cool spiral arms are Kelvin-Helmholtz unstable. In our fiducial simulations, Kelvin-Helmholtz rolls are continually observed for the full 15 orbit duration but can be difficult to discern in the still images of Fig. 1. With higher resolution, the instability becomes more vigorous and discernable. The continual production of Kelvin-Helmholtz rolls leads to mixing and small-scale turbulent velocities in the vicinity of the planet.

Envelope cooling slows as the simulation progresses, such that by the time the simulation ends the cooling rate has dropped by more than an order of magnitude in the deep envelope interior. This fact is reflected in the convergence of profiles in Fig. 2 where the polar temperature profile is plotted every orbit for the fiducial model. Even an exploratory model more than doubling the runtime to 40 orbits shows nearly the same temperature profile (solid black line in Fig. 2).

Notably, this steady cooled profile is distinct from both adiabatic and isothermal cases, though it does remain bounded by the two. Nevertheless, the temperature profile appears similar to what would be obtained from a 1D static model. In Fig. 3 we plot our final simulation temperature profile against one obtained from a symmetric 3D simulation and a 1D static model and find general agreement between the three. In the case of the symmetric 3D simulation, we ran the same model as the fiducial case but starting from a uniform static medium and removing the stratification/rotational source terms. Though this model is not truly symmetric because the box is still Cartesian with various boundaries, inspection indicates that the simulation evolves close to spherical symmetry. The 1D static model is identical to those of Piso & Youdin (2014) but using our static softened potential to be more comparable to the 3D simulations. For the boundary conditions on the static model we take the temperature and pressure at R_b from our symmetric 3D model rather than the unperturbed disk values as our models demonstrate that the planet does still effect disk at this range. While the 1D profile does show minor deviations from the 3D profiles, like a higher central temperature, we believe this is primarily due to the constant luminosity assumption in our 1D model. As in Piso & Youdin (2014), we construct our 1D model

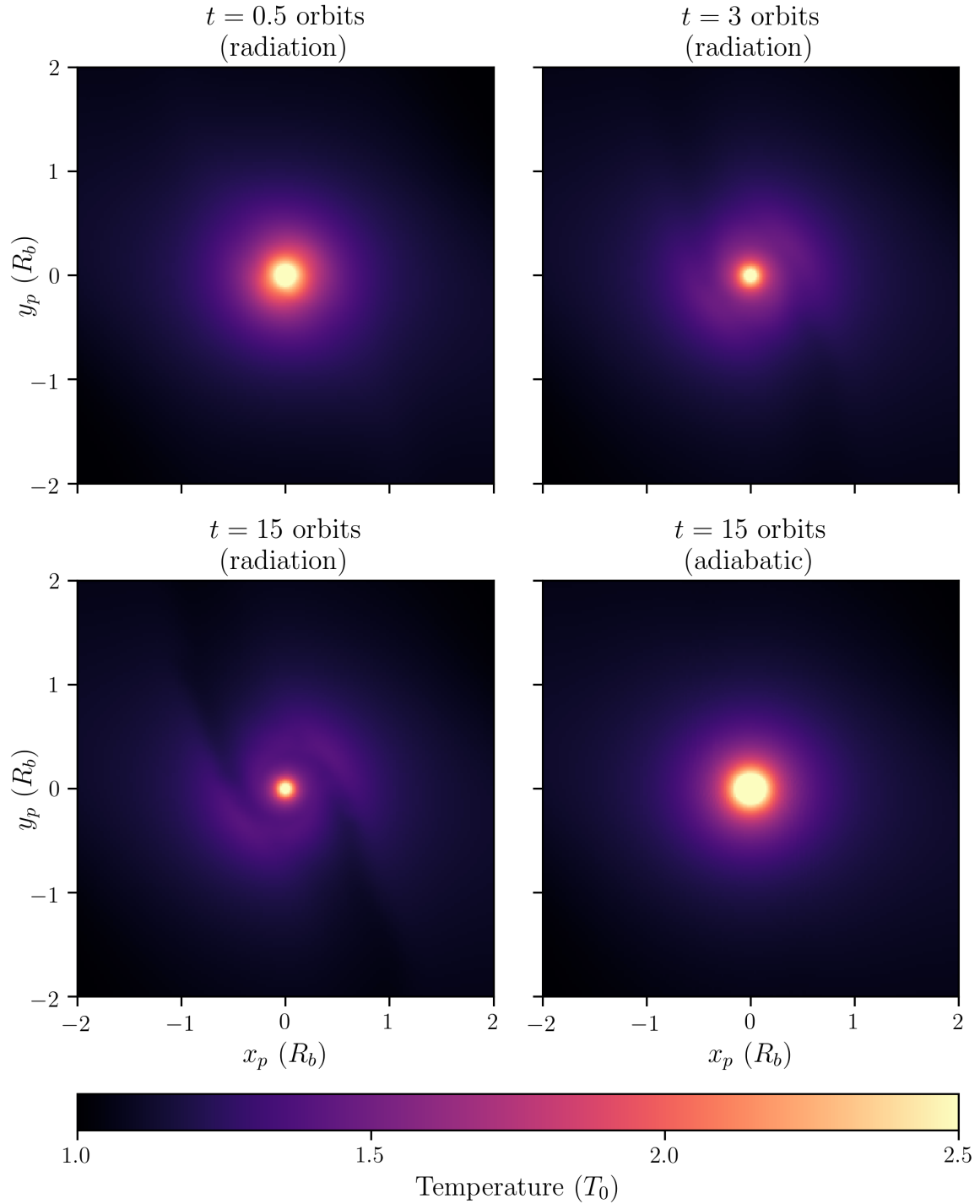


Figure 1. Evolution of the midplane temperature in the fiducial proto-Jupiter simulation. The upper left panel shows the spherically symmetric profile at 0.5 orbits soon after the planet has been introduced. The upper right is a snapshot at 3 orbits. At this point, the envelope has largely adjusted to the planetary potential and radiative cooling is governing the subsequent evolution. The lower left panel shows the further cooled profile after 15 orbits. The lower right panel shows the adiabatic steady state for comparison. Cooled substructures and departures from spherical symmetry are more prominent in radiative models.

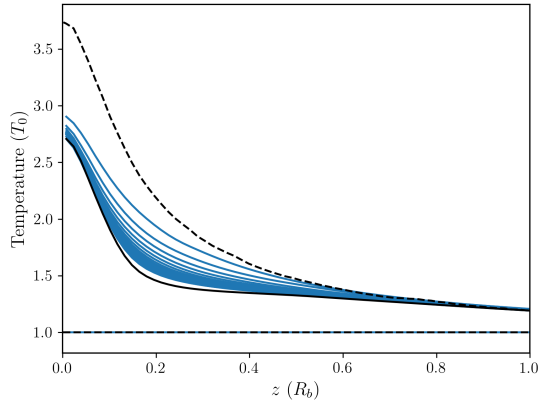


Figure 2. Evolution of the vertical temperature profile for the proto-Jupiter model. Profiles from the fiducial model are sampled along the pole each orbit for 15 orbits and plotted in blue. After an initial heating phase during the introduction of the potential the profiles monotonically cool. We plot the profile from a longer test run at 40 orbits as the solid black line for comparison. Dashed lines show the bounding temperature profiles obtained from corresponding adiabatic and isothermal models.

by making the luminosity constant and tuning it to the exact value as to place the envelope in hydrostatic balance. We plot the luminosities of each model in the lower panel of Fig. 3 and find that temperature profiles diverge as the constant luminosity assumption overestimates the luminosity emerging from the envelope interior. At the same time, the symmetric 1D and 3D models tend to have a much lower luminosity in the envelope outskirts. While this difference manifests weakly in the temperature profile, the higher luminosity indicates that these growing envelopes could be more observable than 1D models predict.

Compared with the temperature profile, the density profile shows a similar pattern of relaxation: the density increases as the atmosphere accretes, all the while maintaining a quasi-static structure. Density profiles also remain bounded by the isothermal and adiabatic profiles. As pointed out in Fung et al. (2019), the envelope masses in adiabatic and isothermal models tend to be lower than necessary for runaway accretion. It seems that this problem persists in radiative models, at least for large softening length. Because models with smaller softening length tend to show greater rotation and rotationally supported envelopes are allowed arbitrary density profiles, it is possible that a rotationally supported radiative model could accrete beyond current model limits. While we have run preliminary models with smaller softening length to address this question, the increased gravitational acceleration seems too large

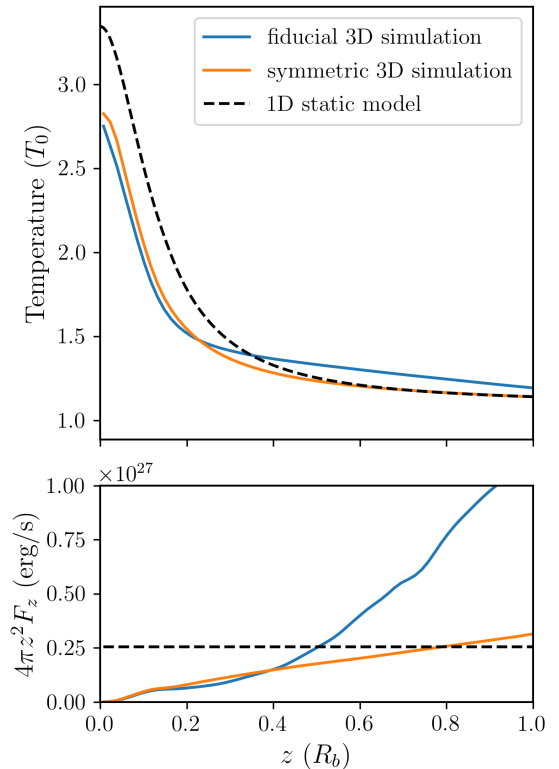


Figure 3. Vertical temperature (top) and luminosity (bottom) of the envelope in our proto-Jupiter model after 15 orbits. The blue curve shows our fiducial simulation. The orange curve is a 3D rad-hydro simulation but treating only the planetary potential so that the simulation is spherically symmetric. The dashed curve is a 1D hydrostatic model assuming a constant luminosity. The luminosity in all cases is calculated using the polar radiative flux F_z assuming spherical symmetry.

to be compatible with our radiation solver at the current resolution.

As cooling of the envelope interior slows, so too does the accretion of gas. We show the rate of change of mass within the Bondi radius as a function of time in Fig. 4. While some of the mass contained within the Bondi radius may be unbound and recycled with the background disk, 1D models treat this as formal size of the envelope, making it a useful as a diagnostic and point of comparison. For the timebeing, we treat this change in mass as an envelope accretion rate as other authors have done but recognize the uncertainty in doing so. By the end of the simulation, this accretion rate has dropped to a rate of $4 \times 10^{-5} M_{\oplus}/\text{yr}$ while the mass inside R_b has leveled out to a value $\approx 0.3M_{\oplus}$. This appears roughly consistent with similar 3D works like Lambrechts et al. (2019) who extrapolate an accretion rate $\approx 10^{-5} M_{\oplus}/\text{yr}$ or Ayliffe & Bate (2009) who find $2 \times 10^{-4} M_{\oplus}/\text{yr}$ for a $10M_{\oplus}$ core.

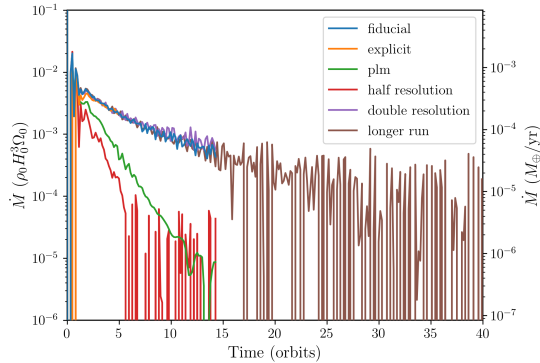


Figure 4. Mass accretion rate within the Bondi sphere as a function of time for models with parameters representative of a proto-Jupiter. The agreement between the fiducial and doubled resolution runs demonstrates the convergence of our fiducial model. Poorly resolved simulations tend to underestimate accretion rates as is evidenced by the half-resolution and piecewise linear (PLM) reconstruction runs.

We validate the fiducial model by running a host of other simulations with different numerical choices. These include: a simulation with the explicit SC radiation method for fewer orbits, a simulation with piecewise linear reconstruction, a simulation with half-resolution everywhere on the grid, a simulation with double-resolution everywhere on the grid, and a longer simulation run for 40 orbits but compensating with a fewer angles per octant. The accretion rates of these test simulations are also plotted in Fig. 4. The good agreement between the fiducial model and the explicit/double-resolution runs suggests that the fiducial model is converged. The PLM and half-resolution runs demonstrate the finding that under-resolved models to underestimate accretion rates. This is consistent with the findings of Schulik et al. (2019), requiring ~ 10 cells per softening length to obtain a converged accretion rate. The accretion rate for the longer run continues to fall but also becomes significantly noisier. The good agreement with the fiducial model at < 15 orbits suggests that at least in this optically thick case, 12 angles per octant more than sufficient for convergence in the optically thick regime.

4. DIVERSITY OF PLANET-FORMING ENVIRONMENTS

While the four parameters q_t , ϵ , κ , β are less intuitive than a parameter like the planet mass they are much more convenient for uniquely defining models. For example, a $10M_{\oplus}$ Jupiter-like core ($T_0 \approx 70$ K, $\Sigma_0 \approx 250$ g/cm 2 , $a \approx 5$ AU, $\kappa \approx 1$ cm 2 /g), could be described by the same model as a $50M_{\oplus}$ planet at $a \approx 100$ AU (with $T_0 \approx 10$ K, $\Sigma_0 \approx 100$ g/cm 2 , $\kappa \approx 2.5$ cm 2 /g) because they share the same q_t , β , κ . Unless of course some other

physics is added, e.g. dissociation of molecules, which sets a temperature scale and breaks this dimensionless scaling.

While the notion of dimensionless parameters simplifies the modelling of forming planets, there must be some connection with the physical dimensional parameters in order to develop an interpretable understanding of planet formation. Here we develop some intuition for how reasonably realistic planets translate to our dimensionless models and vice-versa. This will be useful for the following section where we examine a grid of models spanning a range of different dimensionless parameters. To begin, we can associate dimensionless parameters with disk properties like T_0 , Σ_0 by assuming some reasonable profiles for a protoplanetary disk. For a minimum-mass solar nebula (MMSN) structure, ($\Sigma \propto a^{-3/2}$, $T_0 \propto a^{-1/2}$) the dimensionless parameters then scale with just the physical planet parameters M_p , a and disk opacity κ_0 as:

$$q_t \propto M_p a^{-3/4} \quad (11)$$

$$\kappa \propto \kappa_0(a) a^{-3/2} \quad (12)$$

$$\beta \propto a^{3/2} \quad (13)$$

With some assumed opacity law $\kappa_0(\rho, T)$, the dimensionless parameters can be expressed as solely functions of the readily interpretable parameters a , M_p . This gives some intuition about where in the disk a given model should be applicable. In both 3D and 1D models of planet formation it is typical to adopt the dust grain opacity law of Bell & Lin (1994):

$$\kappa_0 = 2 \left(\frac{T_0}{100 \text{ K}} \right)^2 \text{ cm}^2/\text{g} \quad (14)$$

While widely used for being analytically tractable, this opacity law assumes an interstellar dust-to-gas ratio of 0.01 and is most applicable in cold regions of the disk $T < 100$ K. This gives a scaling for the dimensionless opacity:

$$\kappa \propto a^{-5/2} \quad (15)$$

Notably, κ , β are functions of the disk properties while q_t is a function of both the planet mass and the assumed background disk structure. With this we can map the variation of the two dimensionless parameters β , κ for a given disk model as in Fig. 5. In Fig. 5, we present two curves from reasonable protoplanetary disk models in the (κ, β) plane. Each point on the curves is colored according to its radial location in disk. The two curves adopt different temperature profiles, with the lower one coming from Chiang & Youdin (2010) and the upper one from Rafikov (2006). The scalings are nearly equivalent

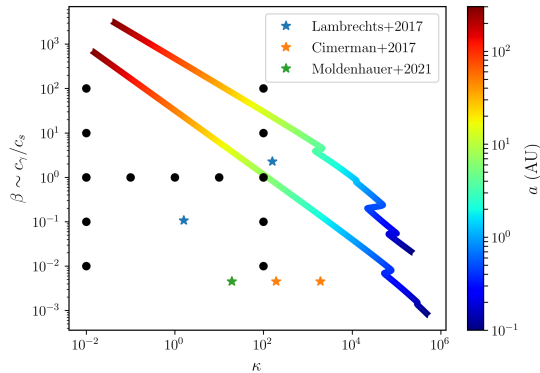


Figure 5. Parameter space of β and κ . Our models are shown as discrete black dots. Colored lines show the trend of parameters as a function radial location in disk for two choices of radial temperature profile in the protoplanetary disk. The parameters of other studies that investigate planets with similar thermal mass are also marked and labelled.

but the upper one is a factor of 2.5 hotter. They both adopt the same MMSN density profile. In the Figure, we drop the convenient analytic opacity of Eq. (14) for Semenov et al. (2003) opacities which include components unique to hotter parts of the disk. Jumps in the opacity law cause the sharp features in hotter opaque regions. The Bell & Lin (1994) law is still reflected in the $\beta \propto \kappa^{-3/5}$ scaling at large $a > 10$ AU where the disk becomes cold. From this plot it is apparent that for a given disk profile, moving outwards in the disk corresponds to larger β and lower κ . Though the precise normalization and slope of this curve can change significantly based upon assumption about opacity, disk mass, etc., the general fact that larger orbital radius corresponds to larger β and lower κ is robust. We also highlight the fact that the spanned parameter space throughout the full disk is rather large, going from optically thick regimes in the inner disk to optically thin in outer disk.

In general, studies employing 3D radiative models tend to focus on a single region of the disk. Usually parameters approximating a prototypical Jupiter or super-Earth are selected and then studied under some variation of either opacity or planet mass. While this is sensible, especially considering the computational cost involved, it makes it considerably harder to compare between models and isolate the role of the local disk conditions T_0 , Σ_0 , κ_0 etc. on the formation process. To this end, in the next section we perform a series of simulations spanning a range of κ and β and study the resulting envelope structure and accretion.

5. A SUITE OF RADIATIVE MODELS

Figure 5 and the preceding estimates suggest that depending on the location in disk, planets could form under a range of conditions from optically thin ($\kappa \ll 1$) to optically thick ($\kappa \gg 1$) but also under a range of β spanning above and below unity. With this in mind, we attempt to cover this (β, κ) parameter space with a set of models that is informative but also computationally feasible. The chosen models are marked in Fig. 5 with circles and correspond to three different branches — an optically thin ($\kappa = 10^{-2}$) branch, an optically thick branch ($\kappa = 10^2$), and a $\beta = 1$ branch. Though this configuration results in models that aren’t necessarily realistic (e.g. $\beta = \kappa = 10^{-2}$), it is convenient from a theoretical perspective, being symmetric about unity and allowing us to test the independent variation of κ and β . At the same time, it does cover realistic regions of parameter space, in many cases overlapping with the work of other studies. By design, our previously presented proto-Jupiter model ($\beta = 1$, $\kappa = 100$) lies directly on this grid, overlapping with the radiative Jupiter-like models by Lambrechts & Lega (2017); Lambrechts et al. (2019); Schulik et al. (2019). Similarly, our ($\beta = 10^{-2}$, $\kappa = 10^2$) model is roughly consistent with the super-Earth conditions adopted by the radiative simulations of Cimerman et al. (2017); Moldenhauer et al. (2021). However, these “super-Earth conditions” assume opacities lower by several orders of magnitude than the Semenov et al. (2003) opacities. This is usually done to hasten cooling and make the problem more computationally tractable while still qualitatively preserving the optically thick formation conditions. For this suite of models we fix the thermal mass to $q_t = 0.5$, a convenient choice applicable to both Jupiter-like cores and super-Earths. The models presented are run for 15 orbits. We also fix the softening length to $\epsilon = 0.1R_b$, consistent with our aforementioned proto-Jupiter model. While this is orders of magnitude too large to represent the core of a Jupiter-like planet, the choice is convenient for the super-Earth case where it would be comparable to the core radius.

5.1. *Optically Thin Models*

5.1.1. *Envelope Structure*

These models, occupying the left vertical branch in Figure 5, are such low opacity that the optical depth through the entire disk even with the planet tends to be less than 1. After 15 orbits, the optically thin temperature profiles range from adiabatic to isothermal depending on the value of β . These temperature profiles are plotted in Fig. 6 in the manner of Fig. 2. The temperature profiles are once again bounded by the adiabatic and isothermal models, becoming more adiabatic for low

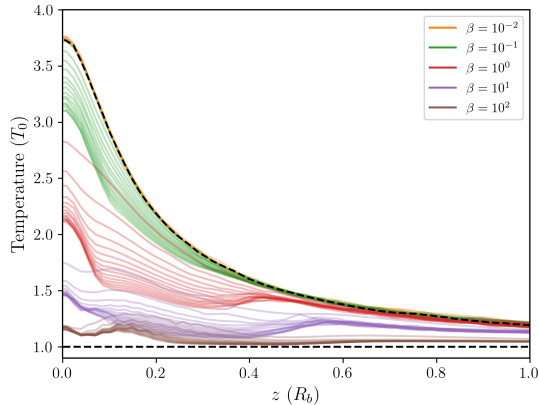


Figure 6. Evolution of vertical temperature profiles along the low-opacity branch. Lines plotted roughly every orbit for 15 orbits. Temperature profiles decrease as atmospheres radiatively cool

β and more isothermal for large β . This ordering can be understood in terms of the optically thin cooling time in a particular model. A thermal perturbation about a homogenous equilibrium solution in an optically thin medium decays at a characteristic rate (Unno & Spiegel 1966):

$$t_{\text{cool}}^{-1} = \frac{c_{\gamma}}{\lambda} \sim \kappa\beta\Omega_0 \quad (16)$$

This suggests that in our optically thin simulations, the ratio of dynamical time to cooling time is simply the product of dimensionless parameters $\kappa\beta$. When the dynamical time and cooling time are roughly equal ($\beta = 10^2$), the envelope is subject to rapid cooling over the course of our 15 orbit simulation and the result is a nearly isothermal temperature profile. For lower values of β , the cooling time becomes longer than the dynamical time and the temperature profile appears increasingly adiabatic.

5.1.2. Mass accretion

The ordering seen in the temperature profiles also manifests in the magnitude of accretion rates. In Fig. 7, we plot the rate of change in mass of the Bondi radius over the simulations' 15 orbits. Whereas the isothermal and adiabatic models reach steady state with accretion rates hovering around zero, optically thin radiative models tend to continually cool and accrete for the full simulation lifetime. The rate at which they accrete mass also appears to be determined by the optically thin cooling rate $\kappa\beta$. Increasing β by an order of magnitude, roughly increases the accretion rate by the same amount. Exceptions to this occur for the lowest value of $\beta = 10^{-2}$ and the highest value of $\beta = 10^2$. The former case has a fairly noisy accretion rate close to zero, similar to the

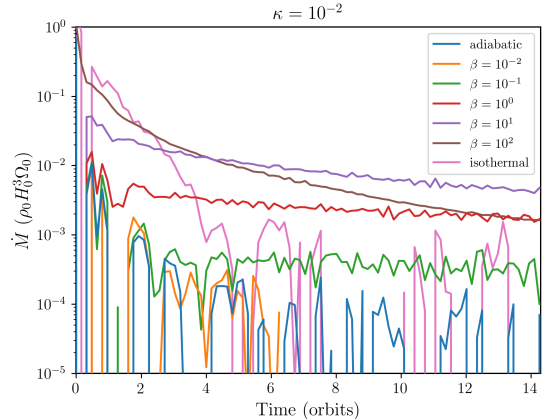


Figure 7. \dot{M} for mass inside Bondi radius as a function of time for models along the optically thin branch.

adiabatic case. The accretion rate in this case may be too low to be distinguishable from noise at this resolution. For $\beta = 10^2$, the radiative timescale and dynamical timescale are comparable making the envelope nearly isothermal. Departures from isothermality still appear great enough to slow the evolution to a still-accreting state by the end of 15 orbits however.

For these optically thin models, we also find that it is not entirely necessary to solve the full transfer equation. By running a set of models with a simple Newtonian cooling prescription, we find good agreement with our fully radiative models when the Newtonian relaxation time was set to the product $\kappa\beta$.

5.2. Optically Thick Models

5.2.1. Envelope Structure

These models, occupying the rightmost branch of Fig. 5 are challenging to run for long as the explicit method timestep becomes prohibitive, particularly as one goes to low β . For this reason, we employ the implicit method for runs with $\beta \leq 1$. As mentioned in the examination of our fiducial proto-Jupiter model, an explicit run is also performed for $\beta = 1$ to confirm that the methods agree in overlapping regions of parameter space. We plot the vertical temperature profiles for this branch in Fig. 8. Similar to the optical thin branch, optically thick models span a range from nearly isothermal to nearly adiabatic depending on their value of β . More than that, for a given value of β , models on the optically thin and optically thick branch relax to similar temperature profiles. The similarity can be understood by considering the optically thick cooling timescale. For a perturbation of wavenumber k on a homogenous optically thick

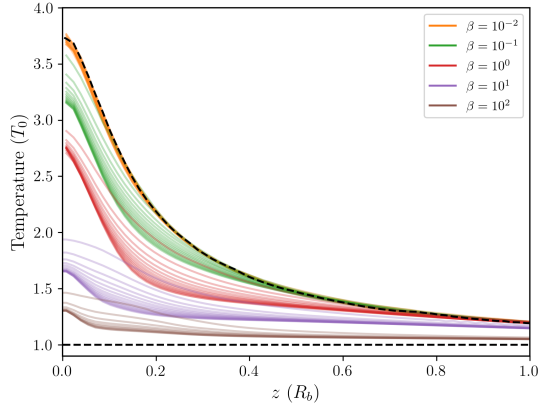


Figure 8. Evolution of vertical temperature profiles along the optically thick branch. Lines plotted roughly every orbit for however long simulation ran. Temperature profiles decrease as atmospheres radiatively cool

medium, the cooling rate is (Unno & Spiegel 1966):

$$t_{\text{cool}}^{-1} = c_{\gamma} k^2 \lambda \sim \frac{\beta k^2}{\kappa \Omega_0} \quad (17)$$

Because the optically thick cooling rate scales as β/κ , a model on our optically thick branch with given β has roughly the same dimensionless cooling time as a model on the optically thin branch with the same β .

5.2.2. Mass accretion

Mass accretion rates for optically thick models (Fig. 9) are roughly similar to their optically thin counterparts, at least in terms of their ordering. However, optically

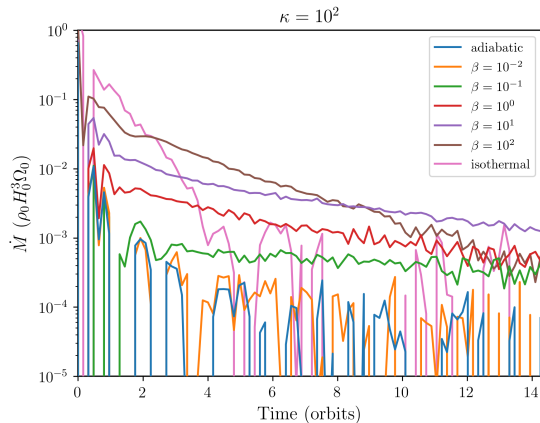


Figure 9. \dot{M} for mass inside Bondi radius as a function of time for various models along the optically thick branch.

thick models with $\beta \geq 1$ show more temporal variation than their optically thin counterparts, decaying by

roughly an order of magnitude over the 15 orbits. The $\beta < 1$ models are nearly identical between the $\kappa = 10^{-2}$ and $\kappa = 10^2$, showing low time-independent accretion rates.

5.3. $\beta = 1$ Models

5.3.1. Envelope Structure

These models are performed at fixed β , but variable opacity. This is more consistent with other studies where the strategy is to usually adopt some fiducial background conditions and then vary the model opacity. In a simple sense, this allows models to parameterize uncertainties associated with dust properties and settling mechanisms in the protoplanetary disk. Unlike the models at fixed κ , these models with identical β share similar vertical temperature profiles which we plot in Fig. 10. The temperature profiles are not ordered monotonically

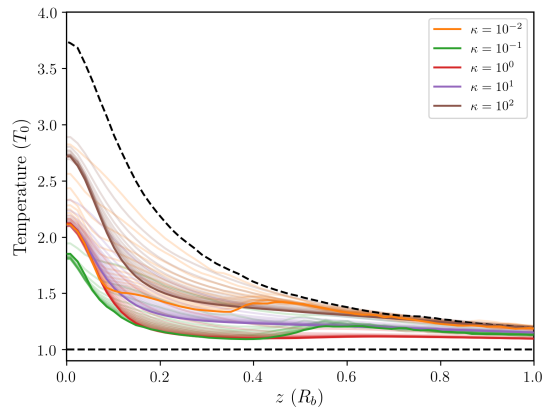


Figure 10. The vertical temperature profiles for models at fixed $\beta = 1$. Unlike Figs. 6 & 8, final profiles are plotted as lines with increased visual opacity to help distinguish between overlapping models.

as they are in optically thick & thin branches. While the most optically thin and optically thick models tend to be slightly hotter, the $\beta = 10^{-2}$ model also matches the onto the temperature profiles of the $\beta = 10^{-1}$ and $\beta = 10^1$ models at small radii. This may be in part due to the softening length as the overlap emerges around $0.1R_b$.

5.3.2. Mass Accretion

Similar to the temperature profiles, mass accretion rates are more clustered than the optically thin and thick branches, suggesting a fairly weak scaling of \dot{M} with κ . As before, we display the accretion rates in the Bondi sphere in Fig. 11. While models with similar cooling times (e.g. $\kappa = 10^{-2}$ and $\kappa = 10^2$) begin accreting at equal rates, once the planet has accrued something

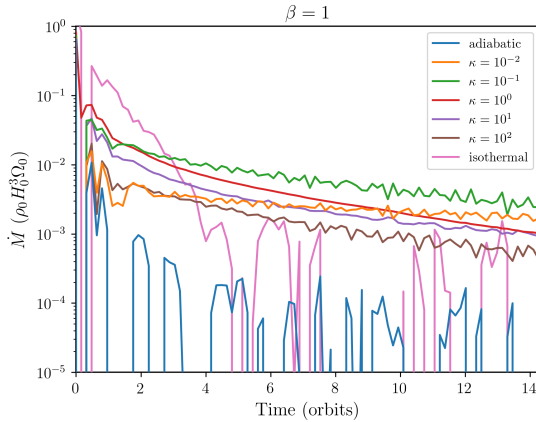


Figure 11. Mass accretion rate at fixed $\beta = 1$ but varying opacity.

of an envelope, the optically thin accretion rates decay more slowly. The result is a higher accretion rate for optically thin models after 15 orbits. While the mass accretion rate does not vary monotonically with opacity because the $\kappa = 10^{-1}$ model has higher accretion rate than $\kappa = 10^{-2}$, the $\kappa = 10^{-1}$ accretion rate is decaying more quickly. If this trend continues, then a monotonic variation of accretion rate with opacity is likely given longer simulation runtimes.

6. DISCUSSION

6.1. Adiabatic or Isothermal?

Depending on the value of β , the models span the space from isothermal to adiabatic temperature profiles by formal end of our simulations. The precise state of gas in the outer envelope is important because the planetary flow field is linked to the assumed gas thermodynamics. Both the character of recycling flows (Kurokawa & Tanigawa 2018) and CPD formation (Fung et al. 2019) can vary greatly depending on the assumed equation of state. The opacity κ does have some minor effect on the outer envelope temperature profiles, with models generally becoming more adiabatic towards higher optical depth. However, the envelope temperature profiles appear to be primarily determined by the choice of model β . While it is colloquially thought that optically thin atmospheres should be isothermal and optically thick atmospheres adiabatic, we demonstrate the existence of optically thick atmospheres with nearly isothermal temperature profiles and rapid cooling. This suggests isothermal models, often discounted for being highly idealized and unrealistic, may occupy some reasonable region of parameter space. Because isothermal models contain robust CPDs, this further suggests that CPDs could exist around low-mass planets, given large enough

β . The models presented here adopt a large softening length, resulting in artificially low rotational velocities and making it difficult to investigate this question of CPD formation. We have run preliminary models with smaller softening length but have encountered numerical issues and departures from symmetry for models along the optically thick branch. Models running along the optically thin branch do suggest the formation of CPDs for $\beta \gtrsim 10$ and disappearance for the more adiabatic looking $\beta \lesssim 1$.

It is standard to take models after several tens of orbits and treat them as representative of the envelope state. Nevertheless, there remains some question of how well this translates to actual planets as the formation process is orders of magnitude longer. 1D static models, having assumed a diffusion approximation everywhere, typically find a more isothermal profile in the outer radiative envelope than the optically thick models run here. This suggests that our models may need to be run longer to truly compare to 1D models. Were we to take these models and continue running them as they are however, we would expect them to simply continue cooling to an isothermal profile ad infinitum. While this is true of something like Jupiter that is still cooling and contracting to this day, it is unrealistic in the sense that the gravity of our planet does not increase with the addition of mass. In the true planet-forming case, the accretion rate would not continue to decrease indefinitely because more massive envelopes accrete at higher rates. Eventually the accretion rate would be so large as to be termed runaway, but our models, being fixed potentials, could never experience a runaway phase. We have also provided no sources of heating either due to planetesimal accretion or an interior envelope in these models. While these would only act to slow the accretion process, their absence also leads to the indefinite cooling of our models. In the future, we hope to improve our models by imposing a luminosity near the softening length to represent the subgrid interior envelope. Depending on the cooling time, the heated outer envelope would presumably come to a steady state and could be compared more directly with static 1D models.

6.2. Accretion Rates

While we have presented model accretion rates in the preceding sections, we do not regard these as actual planetary accretion rates. For one, these are the accretion rates of mass within the planet’s Bondi radius and there is no guarantee that all of this mass remains bound to the planet. Furthermore, the mass accretion rates have a tendency to decrease with time, suggesting that accretion rates could be made lower by sim-

ply adopting a longer runtime. For these reasons we do not treat the presented rates as indisputable but rather as upper bounds on some true planetary accretion rate so long as the simulations are converged. Though our models also adopt a larger softening length than is realistic for most planets, the results of [Schulik et al. \(2019\)](#) suggest that going to smaller softening length only decreases the corresponding accretion rates. In particular, lowering the softening length creates a deeper potential thereby raising the energy content of the envelope. While the luminosities also increase, it is not in keeping with the energy content, resulting in a lower net mass accretion rate. This suggests that the interpretation of our model accretion rates as an upper bound is robust.

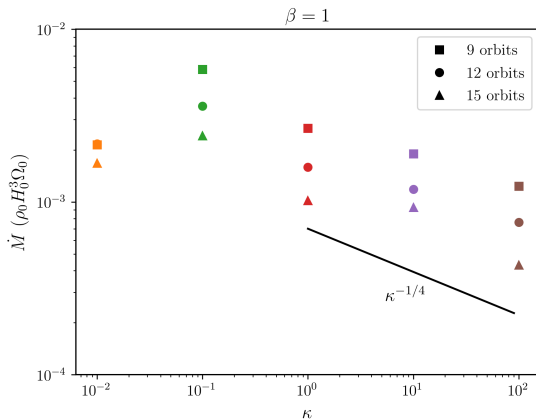


Figure 12. Accretion rates as a function of model opacity. Points are sampled three times from the simulation at 9 orbits (squares), 12 orbits (circles) and 15 orbits (triangles). We find that accretion scale as roughly $\kappa^{-1/4}$, with $\kappa = 10^{-2}$ being a potential exception.

Without being certain of the true planetary accretion rate, we are still in a position to make relative comparisons between the presented models and extend these to more physical scenarios. In particular, we can infer from our $\beta = 1$ branch some estimate of how the mass accretion rate varies with opacity. When we plot the \dot{M} as a function of κ for these models (Fig. 12), we find an approximate $\kappa^{-1/4}$ scaling consistent with similar 3D radiation-hydrodynamics studies that overlap our optically thick cases ([Ayliffe & Bate 2009](#); [Schulik et al. 2019](#)). We do find that our most optically thin model shows a departure from this scaling but due to the limited sampling in κ it is difficult to tell how robust this is. Also because the mass accretion rate in the $\kappa = 10^{-2}$ model exhibits less rapid decay than all the other models, it is also likely that points sampled from a longer simulation run would be more in accordance with the

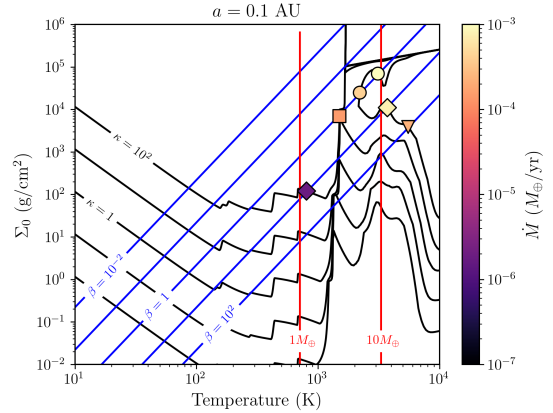


Figure 13. Dimensional mass accretion rates at 0.1 AU as a function of disk surface density and disk temperature. Black lines are contours of $\kappa = [10^{-2}, 10^{-1}, 10^0, 10^1, 10^2]$ assuming [Semenov et al. \(2003\)](#) opacities for $\kappa_0(\rho_0, T_0)$. Blue lines are contours of $\beta = [10^{-2}, 10^{-1}, 10^0, 10^1, 10^2]$. The rightmost red line marks a $10M_{\oplus}$ core and the left line a $1M_{\oplus}$ core. At the contour intersections for particular values of κ and β we are able to apply and dimensionalize our dimensionless model which we show with markers colored according to the model accretion rate.

$\kappa^{-1/4}$ scaling. The $\kappa^{-1/4}$ scaling is distinct from 1D models that predict a scaling closer to $1/\kappa$ ([Ikoma et al. 2000](#)). Other studies investigating higher mass planets have found the κ dependence continues to weaken as the accretion becomes disk-limited ([D’Angelo & Bodenheimer 2013](#)). While it has been suggested that $\kappa^{-1/4}$ is simply an intermediate regime lying between the 1D and disk-limited rates, our models here are low enough mass ($10M_{\oplus}$) as to overlap with the 1D regime. This suggests a more fundamental difference between the 1D and 3D models that we hope to investigate in the future by directly comparing with 1D models. Other studies with this sub-linear opacity scaling have suggested that the dependence could be reflective of model initial conditions as their methodology changes the initial disk mid-plane density and opacity simultaneously ([Schulik et al. 2019](#)). Because we use a local box with the same initial conditions independent of opacity, our simulations suggest that this scaling is more robust and we are at least able to rule out that hypothesis in the meantime.

For some set of conditions in the disk, like $(\rho_0, T_0, \kappa_0, a)$, it is possible to dimensionalize our models and study mass accretion throughout the disk. Because we choose a fixed thermal mass $q_t = 0.5$, the planet mass of a given model is fixed by choosing a disk temperature T_0 and an orbital radius a . While it is unfortunate that we may not vary a planet’s mass and disk conditions independently, we have chosen q_t in particular to be applicable to both proto-Jupiter and super-Earth conditions.

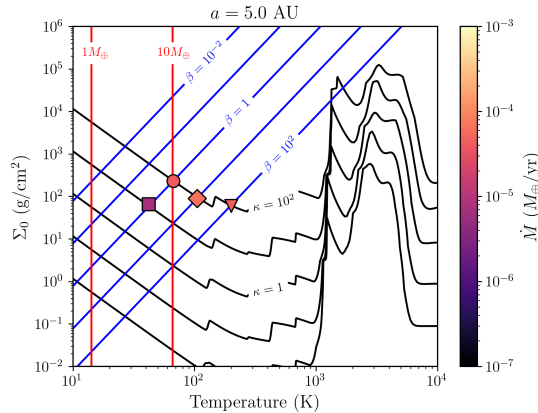


Figure 14. Dimensional mass accretion rates at 5.0 AU as a function of disk surface density and disk temperature plotted in the style of Fig. 13. Models sharing the same dimensionless (β, κ) are plotted with the same symbol between this figure and Fig. 13.

Dimensionalizing also requires some choice of the opacity κ_0 which we take to be the temperature and density dependent opacities of Semenov et al. (2003). While this is not entirely self-consistent as the models themselves were simulated with a temperature and density independent opacity, it is more informative than arbitrarily choosing some constant opacity. With $\kappa_0(\rho_0, T_0)$, we can choose a location in the disk a , a density ρ_0 , and a temperature T_0 and calculate the dimensionless (β, κ) . In Figs. 13 & 14, we invert this process, taking our models which have a fixed (κ, β) and finding the (ρ_0, T_0) that these models could represent in a physical disk. We then dimensionalize the mass accretion rate and plot them as a function of (Σ_0, T_0) . Fig. 13 corresponds to the choice of $a = 0.1$ AU and as the points lie roughly in the $1 - 10M_{\oplus}$, $T_0 \sim 1000$ K, $\Sigma_0 \sim 10^5$ g/cm² region, they are indeed super-Earth like. Fig. 14 corresponds to the choice of $a = 5.0$ AU and models are applicable to Jupiter-like conditions at $T_0 \sim 100$ K, $\Sigma_0 \sim 100$ g/cm².

With the dimensional accretion rates in Figs. 13 & 14, we notice that the magnitude of accretion rates is large enough such that all models would be able to accrete an envelope comparable to their core mass within a disk lifetime ($t \sim 10^6$) and potentially enter a runaway stage of growth. However this quoted accretion rate is only representative of the earliest phases of planet growth. On scales longer than the simulated time here and for most of the protoplanet’s lifetime, we expect the accretion rate to be significantly lower. In order to estimate the true accretion rate for the pre-runaway lifetime it becomes necessary to construct a 1D model consistent with and informed by the 3D simulation in the regime where they overlap and then evolve the 1D on longer

timescales. Rather than do this here, we refer to an additional paper (Bailey & Zhu 2023) focused on adequately parameterizing the effects of 3D recycling into 1D models. Here instead we focus on the model setup, fidelity, details, and dimensionless framework.

6.3. Validity of Radiative Transfer Approximations

In previous sections, we remarked on and showed some evidence of the agreement between the implicit/explicit methods. Because the explicit method neglects the time derivative of I and any velocity dependent terms in the solution of the radiation field, it is a static approximation. In particular, fluid motion must occur more slowly than the time it takes radiation to diffuse or free stream. The implicit method on the other hand solves the full velocity-dependent transfer. Due to the good agreement between the two methods we can conclude that static methods are perfectly viable and computation of velocity dependent terms is extraneous for these types of models.

Because we utilize methods that solve the transfer equation instead of a closure approximation, we are also in a position to evaluate the fidelity of radiative approximations commonly employed by other studies. The simplest cooling model is a Newtonian linear cooling law, applicable to optically thin regions. For our optically thin $\kappa = 10^{-2}$ models, we find remarkable agreement with a simple linear cooling law. Fig. 15 shows a comparison of the sliced temperature profiles of two optically thin models, one solving the full transfer equation and one applying linear cooling as an energy source term. So long as the linear cooling rate is set appropriately ($t_{\text{cool}} \sim \kappa\beta$), we find similar agreement for all models on our optically thin branch. While this is convenient because a linear cooling law adds negligible computational cost, the applicability to planet simulations is rather slim. As suggested by Fig. 5, only at large orbital radius (i.e. low surface density) is optically thin reasonable and even then the density increase near the planet can make some part of the envelope optically thick. For that reason, this method is only really tenable when focused on an optically thin outer envelope or only interested in a toy model for envelope cooling e.g. Kurokawa & Tanigawa (2018).

Though we can’t explicitly perform FLD runs as it is not currently implemented in ATHENA++, we are able to examine the true fluxes and determine if they are consistent with a diffusion approximation. In Fig. 16, we plot the mean intensity (radiation energy density up to a constant) for several different opacity models on the $\beta = 1$ branch. Direction vectors for the radiation flux and also the gradient of the energy density ∇E_r are

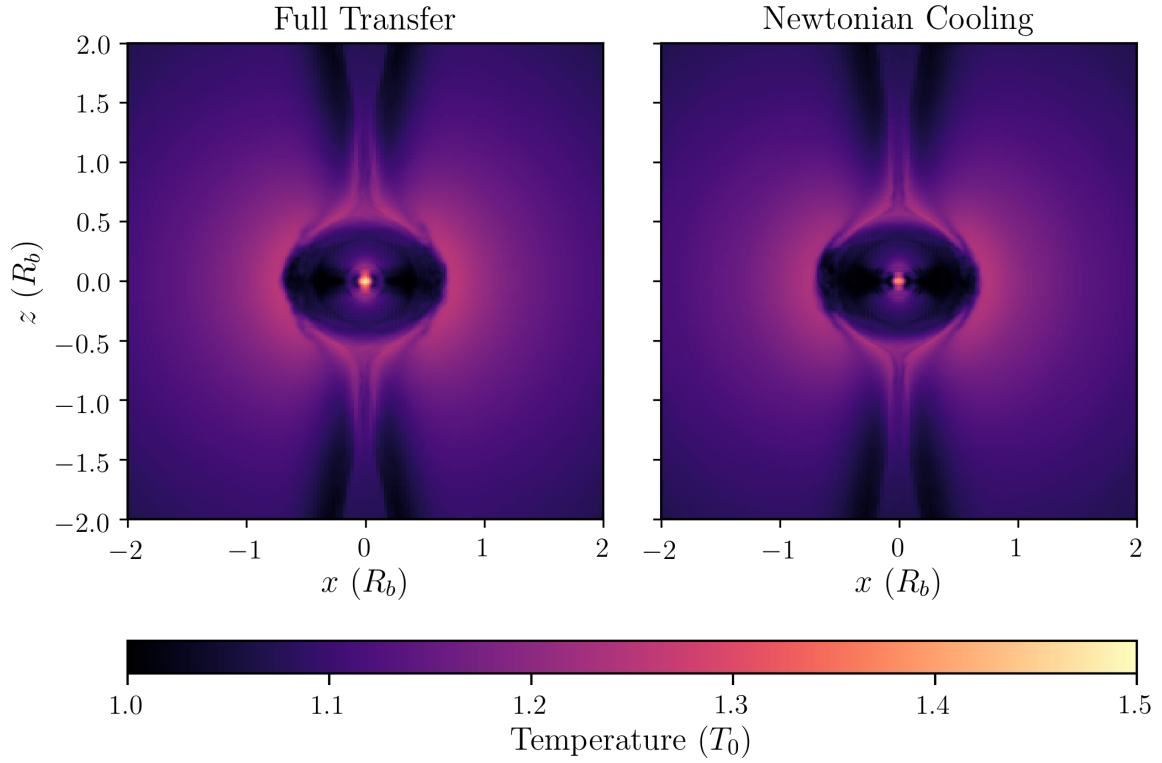


Figure 15. Vertically sliced temperature profiles after 15 orbits for the optically thin $\beta = 10$ model. The left panel comes from a simulation employing our full radiative transfer module whereas the right panel simply applies a linear cooling law as a source term to the energy equation.

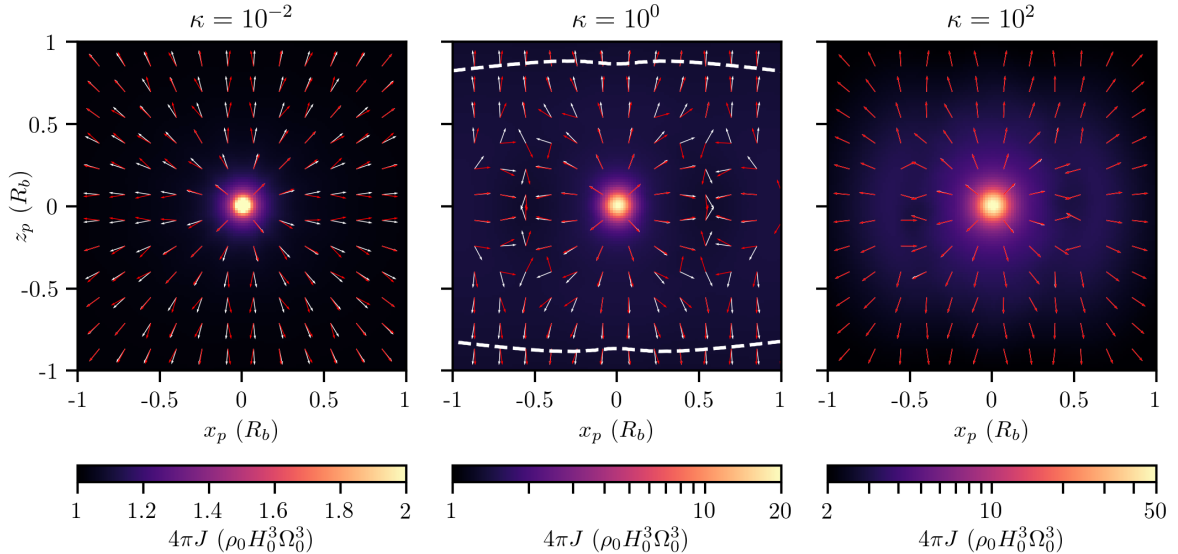


Figure 16. Vertically sliced profiles of the radiation field for different opacity models. Slices are colored according to the mean intensity J . White vectors show the true radiation flux while red vectors show the gradient of the radiation energy density. All are unit vectors and not representative of the magnitude. The dashed line marks the location of vertical optical depth $\tau = 1$. While $\kappa = 10^{-2}$ is too optically thin to reach unity optical depth, the $\tau = 1$ surface for $\kappa = 10^2$ lies outside the range of the plot at a height of nearly $4R_b$.

also shown and match very well for the optically thick model. For the optically thin model, while vectors don't match as perfectly, both the flux and the energy density gradient are nearly radial. In the intermediate $\kappa = 1$ case, the fluxes are no longer radial, showing interesting deviations based on temperature variations in the planetary envelope. While the fluxes and ∇E_r can be largely misaligned in certain areas of the envelope, the vectors end up being roughly aligned and largely vertical on the scale of the photosphere. This suggests that FLD, particularly in the optically thick models should be fairly reasonable. Considering that solution of the transfer equation tends to add 1-2 orders of magnitude in computation time depending on the number of angles per cell, we recommend the use of FLD for this application. In particular, we believe the advantages offered by going to higher resolution and longer runtimes far outweigh the benefits offered by more accurate radiative transfer.

7. SUMMARY

We have carried out a range of hydrodynamics simulations of envelopes around planetary cores employing a solution of the full radiative transfer equation. We formulate the problem in terms of dimensionless parameters κ , β , q_t , and ϵ (Sec. 2). Simulations were performed for a variety of κ and β corresponding to different disk conditions and optical depths ranging from optically thin to optically thick. With these simulations we were able to obtain profile for envelope structure and mass accretion rates or at least upper limits on the minimum accretion rate. We list some of our findings:

- Planet envelopes with radiative cooling are neither adiabatic nor isothermal. Precisely how adiabatic or isothermal they are is not solely a function of opacity but is primarily determined by β , related to the cooling time.

- Models show a weak $\kappa^{-1/4}$ scaling of accretion rate well below the disk-limited accretion regime. This is less steep than reported by 1D evolutionary models at similar stages.
- We have obtained upper-limits to 3D mass accretion rates prior to runaway growth for a wide range of parameters. This corresponds to lower-limits on the formation timescale or time to reach crossover mass. The rates are dimensionalized for proto-Jupiters and super-Earth like formation conditions in Figs. 13 & 14.
- Flux limited diffusion is a reasonable method for simulating planetary envelopes, particularly when one considers the cost savings over more sophisticated methods.

ACKNOWLEDGMENTS

The authors are also pleased to acknowledge that the work reported on in this paper was substantially performed using the Princeton Research Computing resources at Princeton University which is consortium of groups led by the Princeton Institute for Computational Science and Engineering (PICSciE) and Office of Information Technology's Research Computing.

The simulations presented in this article were performed on computational resources managed and supported by Princeton Research Computing, a consortium of groups including the Princeton Institute for Computational Science and Engineering (PICSciE) and the Office of Information Technology's High Performance Computing Center and Visualization Laboratory at Princeton University.

REFERENCES

- Auer, L. H., & Paletou, F. 1994, *A&A*, 285, 675
- Ayliffe, B. A., & Bate, M. R. 2009, *MNRAS*, 397, 657, doi: [10.1111/j.1365-2966.2009.15002.x](https://doi.org/10.1111/j.1365-2966.2009.15002.x)
- . 2012, *MNRAS*, 427, 2597, doi: [10.1111/j.1365-2966.2012.21979.x](https://doi.org/10.1111/j.1365-2966.2012.21979.x)
- Bailey, A. P., & Zhu, Z. 2023
- Bell, K. R., & Lin, D. N. C. 1994, *ApJ*, 427, 987, doi: [10.1086/174206](https://doi.org/10.1086/174206)
- Chiang, E., & Youdin, A. N. 2010, *Annual Review of Earth and Planetary Sciences*, 38, 493, doi: [10.1146/annurev-earth-040809-152513](https://doi.org/10.1146/annurev-earth-040809-152513)
- Cimerman, N. P., Kuiper, R., & Ormel, C. W. 2017, *MNRAS*, 471, 4662, doi: [10.1093/mnras/stx1924](https://doi.org/10.1093/mnras/stx1924)
- D'Angelo, G., & Bodenheimer, P. 2013, *ApJ*, 778, 77, doi: [10.1088/0004-637X/778/1/77](https://doi.org/10.1088/0004-637X/778/1/77)
- Davis, S. W., Stone, J. M., & Jiang, Y.-F. 2012, *ApJS*, 199, 9, doi: [10.1088/0067-0049/199/1/9](https://doi.org/10.1088/0067-0049/199/1/9)
- Fung, J., Artymowicz, P., & Wu, Y. 2015, *ApJ*, 811, 101, doi: [10.1088/0004-637X/811/2/101](https://doi.org/10.1088/0004-637X/811/2/101)
- Fung, J., Zhu, Z., & Chiang, E. 2019, *ApJ*, 887, 152, doi: [10.3847/1538-4357/ab53da](https://doi.org/10.3847/1538-4357/ab53da)

- Ikoma, M., Nakazawa, K., & Emori, H. 2000, *ApJ*, 537, 1013, doi: [10.1086/309050](https://doi.org/10.1086/309050)
- Jiang, Y.-F. 2021, *ApJS*, 253, 49, doi: [10.3847/1538-4365/abe303](https://doi.org/10.3847/1538-4365/abe303)
- Kunasz, P., & Auer, L. H. 1988, *JQSRT*, 39, 67, doi: [10.1016/0022-4073\(88\)90021-0](https://doi.org/10.1016/0022-4073(88)90021-0)
- Kurokawa, H., & Tanigawa, T. 2018, *MNRAS*, 479, 635, doi: [10.1093/mnras/sty1498](https://doi.org/10.1093/mnras/sty1498)
- Lambrechts, M., & Lega, E. 2017, *A&A*, 606, A146, doi: [10.1051/0004-6361/201731014](https://doi.org/10.1051/0004-6361/201731014)
- Lambrechts, M., Lega, E., Nelson, R. P., Crida, A., & Morbidelli, A. 2019, *A&A*, 630, A82, doi: [10.1051/0004-6361/201834413](https://doi.org/10.1051/0004-6361/201834413)
- Melon Fuksman, J. D., Klahr, H., Flock, M., & Mignone, A. 2021, *ApJ*, 906, 78, doi: [10.3847/1538-4357/abc879](https://doi.org/10.3847/1538-4357/abc879)
- Moldenhauer, T. W., Kuiper, R., Kley, W., & Ormel, C. W. 2021, *A&A*, 646, L11, doi: [10.1051/0004-6361/202040220](https://doi.org/10.1051/0004-6361/202040220)
- Ormel, C. W., Shi, J.-M., & Kuiper, R. 2015, *MNRAS*, 447, 3512, doi: [10.1093/mnras/stu2704](https://doi.org/10.1093/mnras/stu2704)
- Piso, A.-M. A., & Youdin, A. N. 2014, *ApJ*, 786, 21, doi: [10.1088/0004-637X/786/1/21](https://doi.org/10.1088/0004-637X/786/1/21)
- Rafikov, R. R. 2006, *ApJ*, 648, 666, doi: [10.1086/505695](https://doi.org/10.1086/505695)
- Schulik, M., Johansen, A., Bitsch, B., & Lega, E. 2019, *A&A*, 632, A118, doi: [10.1051/0004-6361/201935473](https://doi.org/10.1051/0004-6361/201935473)
- Semenov, D., Henning, T., Helling, C., Ilgner, M., & Sedlmayr, E. 2003, *A&A*, 410, 611, doi: [10.1051/0004-6361:20031279](https://doi.org/10.1051/0004-6361:20031279)
- Szulágyi, J. 2017, *ApJ*, 842, 103, doi: [10.3847/1538-4357/aa7515](https://doi.org/10.3847/1538-4357/aa7515)
- Unno, W., & Spiegel, E. A. 1966, *PASJ*, 18, 85
- Zhu, Z., Bailey, A., Macías, E., Muto, T., & Andrews, S. M. 2023, *MNRAS*, 518, 5808, doi: [10.1093/mnras/stac2668](https://doi.org/10.1093/mnras/stac2668)
- Zhu, Z., Jiang, Y.-F., Baehr, H., et al. 2021, *MNRAS*, 508, 453, doi: [10.1093/mnras/stab2517](https://doi.org/10.1093/mnras/stab2517)